Polymer 280 (2023) 126064

Contents lists available at ScienceDirect

Polymer

journal homepage: www.elsevier.com/locate/polymer

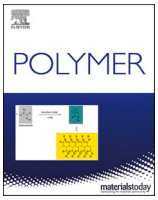

Poly(diallylmethylammonium) proton conducting membranes with high ionic conductivity at intermediate temperatures

Antonela Gallastegui [a,**], Fabrizia Foglia [b], Paul F. McMillan [b], Nerea Casado [a,d], Aurelie Gueguen [c,***], David Mecerreyes [a,d,*]

[a] POLYMAT, University of the Basque Country UPV/EHU, Avenida Tolosa 72, Donostia-San Sebastian, 20018, Gipuzkoa, Spain
[b] Department of Chemistry, Christopher Ingold Laboratory, University College London, London, WC1H 0AJ, UK
[c] Material Engineering Division, Toyota Motor Europe NV/SA, Technical Center, 1930, Zaventem, Belgium
[d] IKERBASQUE, Basque Foundation for Science, Bilbao, Spain

ARTICLE INFO

Keywords:
Protic ionic liquids
Diallylmethylammonium polymers
Proton conducting membranes
PEM
Hydrogen fuel cells

ABSTRACT

High temperature proton exchange membrane fuel cells are being lately investigated because of their high energy efficiency, their superior heat/water management, CO tolerance, and electrode reaction kinetics. To further advance this technology, the polymer membrane portfolio and performance should be improved for intermediate or high temperature operation (>100 °C). In this work we present new poly(diallylmethylammonium) proton conducting membranes with high ionic conductivity at 120 °C. First, new protic ionic liquids, hereafter called $DAMAH^+X^-$, were synthesized leading to diallylmethylammonium monomers with different counter-anions. By radical cyclopolymerization through thermal and photoinitiation mechanisms, self-standing protic polymeric membranes of poly(diallylmethylammonium X^-) were obtained. Membranes showed good thermal stability (>250 °C) and mechanical properties without the need of additives such as (protic) ionic liquids, solvents or inorganic charges. Great attention was paid to understand the effect of the different counter-anions on the membrane properties. As a general trend, fluorinated anions coming from strong acids confer high ionic conductivity and allow to reduce the hygroscopic properties on the protic polymeric membranes. Proton structural and dynamical stability at different temperatures and humidification conditions were investigated by Neutron Scattering (QENS and NR). The optimized poly(diallylmethylammonium X^-) shows similar ionic conductivity values than Nafion 212 under varying relative humidity conditions at 80 °C. Furthermore, it shows a high ionic conductivity value of 1.9×10^{-3} S cm^{-1} at 120 °C under dry conditions.

1. Introduction

Nowadays, proton exchange membrane fuel cells (PEMFCs) are considered to be a highly efficient and clean technology for energy conversion due to high energy/power densities, low/zero emission operation, silent operation and broad range of applications [1–3]. Three major types of hydrogen PEMFCs are currently being investigated, designed to operate at i) low (<80 °C); ii) intermediate (80–120 °C aprox.), and iii) high temperatures (120–200 °C) [4]. Particular attention is being developed around intermediate or high temperature PEMFCs (IT-PEMs) because of their superior heat/water management regarding easier heat dissipation and potentially elimination of PEM hydration, good CO tolerance, and enhanced electrode reaction kinetics [4–6]. Although improved FC performances are usually achieved at high relative humidity, in the case of IT-PEM, operation use at lower relative humidity (RH) is desirable because of the higher saturated vapour pressure at 120 °C [4].

Nowadays perfluorinated sulfonic acid (PFSA) membranes, like Nafion, are the most common membranes used in low temperature PEMFCs systems due to their high performances and lifetime [7,8]. Nevertheless, several non-fluorinated polymer alternatives have been developed to overcome the drawbacks inherent to PFSA membranes,

* Corresponding author. POLYMAT, University of the Basque Country UPV/EHU, Avenida Tolosa 72, Donostia-San Sebastian, 20018, Gipuzkoa, Spain.
** Corresponding author.
*** Corresponding author.
E-mail addresses: antonela.gallastegui@polymat.eu (A. Gallastegui), f.foglia@ucl.ac.uk (F. Foglia), p.f.mcmillan@ucl.ac.uk (P.F. McMillan), nerea.casado@ehu.eus (N. Casado), aurelie.gueguen@toyota-europe.com (A. Gueguen), david.mecerreyes@ehu.es (D. Mecerreyes).

https://doi.org/10.1016/j.polymer.2023.126064
Received 6 February 2023; Received in revised form 19 May 2023; Accepted 27 May 2023
Available online 30 May 2023

mainly high cost, high gas crossover and restricted operation under anhydrous conditions [9–12]. Thus, a common problem associated with PFSA membranes is the drastic loss of proton conductivity at temperatures >100 °C due to the membrane dehydration. Therefore, proton-conducting materials that exhibit high proton conductivity, superior thermal/electrochemical stability and good mechanical properties above 100 °C are actively searched [1]. Developments in this direction include modified PFSA membranes, sulfonated hydrocarbon polymers membranes, phosphoric acid doped polybenzimidazole membranes or acid base membranes (doped membranes with ionic liquids) [4,13]. The low proton conductivity, the poor mechanical properties, insufficient thermal stability and, most of the times, the presence of free added acids that may evaporate or degrade the membrane, are common drawbacks when designing PEMs with optimal performance at high temperatures [14–16]. Furthermore, the increasing interest in green hydrogen production technologies using electrolysers is also showing the need of new membranes for high temperature operation.

An approach to design new PEMs is to adapt the chemistry of protic ionic liquids to new polymers [3,17,18]. Protic ionic liquids have recently attracted much attention since they exhibit high proton conductivity around 10^{-2} and 10^{-3} S cm^{-1} at temperatures >100 °C and under anhydrous conditions [2,19–21]. Moreover, they exhibit high thermal and electrochemical stabilities, with a degradation temperature about 200–300 °C and a width operational electrochemical window [22–27]. As an illustrative example, Isik et al. synthesized protic poly (ionic liquid)s employing commercial phosphonium counter-cations achieving high dry ionic conductivity of 2×10^{-4} S cm^{-1} at 150 °C [28]. In another study, Rao et al. developed novel proton conducting ionogels based on a non-protic poly(ionic liquid) host and 60 wt% of a free protic ionic liquid, N,N-diethylmethylammonium triflate, leading to a membrane that presented a high ionic conductivity of 5.8×10^{-3} S cm^{-1} at 100 °C [27]. Another good example is the recent work carried out by Huang et al., in which they increased the ionic conductivity of a polystyrene type protic poly(ionic liquid) with the incorporation of protic ionic liquids with similar chemical structure as the polymer, presenting a conductivity of 5×10^{-3} S cm^{-1} at 120 °C [29]. These previous works indicate the promising strategy of developing proton conducting membranes based on protic poly(ionic liquid)s with high ionic conductivity at temperatures higher than 100 °C.

Among the different poly(ionic liquid)s investigated in energy applications, cationic poly(diallyldimethylammonium) (PDADMA) backbone in combination of different anions has shown superior mechanical and electrochemical properties. As one illustrative example, the work presented by Huang et al. in which they mixed PDADMA with protic ionic liquids to develop self-standing composite PEMs [30–32]. For these reasons, PDADMA poly(ionic liquid)s have been actively investigated in different applications such as binders for battery electrodes or polymer electrolyte membranes for lithium or sodium batteries [30,32]. As an alternative in this work, we present the synthesis of new protic poly(diallylmethylammonium X^-) PDAMAH$^+$X$^-$ polymers and their properties as high conducting membranes for intermediate temperature. For this purpose, seven new protic ionic liquid monomers were synthesized based on diallylmethylammonium cation and different fluorinated and non-fluorinated anions. The synthesis of protic monomers, instead of the usually direct polymer protonation offers polymer design possibilities and ensures full protonation. Next, for the first time, free radical cyclopolymerization of these new monomers using thermal initiators and photoinitiators was investigated. The protic PDAMAH$^+$X$^-$ PEMs were processed as free-standing membranes and their thermal stability, ionic conductivity and, for some of them, mechanical and humidity uptake properties were studied. Particular attention was paid to understand the effect of the different counter-anions on the membrane properties and the proton conduction at intermediate temperatures.

2. Experimental section

2.1. Materials

Diallylmethylamine (DAMA, 98%) was bought from Acros Organics. Phosphoric acid (H_3PO_4, 99%, 85 wt% in H_2O), sulfuric acid (H_2SO_4, 95–98%), hydrochloric acid (HCl, 37 wt% in H_2O), trifluoromethanesulfonic acid (HTf, 97%), methanesulfonic acid (MSA, 99,99%), triallylamine (TAA, 99%) and bis(trifluoromethanesulfonyl) imide acid (HTFSI, 95%) were purchased from Sigma Aldrich. Thermal initiators, 2,2′-azobis(2-methylpropionamide)dihydrochloride (AIBA) and N,N′-azobisisobutyronitrile (AIBN), and the UV photoinitiator 2-hydroxy 2-methylpropiophenone (Darocur 1173, 97%) were purchased from Sigma Aldrich. Acetonitrile (ACN) was obtained from Fisher. All reagents were employed with no further purification.

2.2. Preparation of new polymerizable protic diallylmethylammonium (DAMAH$^+$X$^-$) ionic liquids

Protic ionic liquid monomers, DAMAH$^+$ $H_2PO_4^-$, DAMAH$^+$Cl$^-$, DAMAH$^+$ HSO_4^-, DAMAH$^+$MsO$^-$, DAMAH$^+$Tf$^-$, and DAMAH$^+$TFSI$^-$, were synthesized by reacting diallylmethylamine (DAMA) with the corresponding inorganic/organic acid. To this end, each acid was added dropwise slowly to DAMA under agitation in a ratio 1:1 mol and left during 24 h to form the protic ionic liquid. As shown on Scheme 1, one H^+ is exchanged from the acid to the monomer DAMA, creating the protic ionic liquid. As shown also in the scheme, a protic ionic liquid based on triallylamine (TAA) and methanesulfonic acid (MSA), TAAH$^+$MsO$^-$, was also synthesized for its use as a crosslinker. All the synthesized compounds were characterized to confirm their structure and properties through ^{1}H NMR, FTIR, TGA and ionic conductivity.

2.3. Synthesis of protic poly(ionic liquids) through thermal and photopolymerization

PDAMAH$^+$X$^-$ were prepared by thermal polymerization using 2,2′-azobis(2-methylpropionamide)dihydrochloride (AIBA) initiator or N,N′-azobisisobutyronitrile (AIBN) (depending on the hydrophilicity of the protic ionic liquid). DAMAH$^+$ $H_2PO_4^-$, DAMAH$^+$ HSO_4^-, DAMAH$^+$Cl$^-$, DAMAH$^+$MsO$^-$ and DAMAH$^+$Tf$^-$ were deoxygenated for 30 min in water (30 wt%) and stirred at 70 °C together with AIBA (3 wt% with respect to the protic ionic liquid monomers) in water for 24 h. In the case of DAMAH$^+$TFSI$^-$, the polymerization procedure was the same as the other protic ionic liquids but instead of water, ACN was employed. A dialysis step was then carried out to purify the obtained polymers and ensure removal of unreacted protic ionic liquid monomers. Each liquid mixture was then poured into a silicon mold and left dry for 24 h at 70 °C to obtain the final membrane.

Protic PDAMAH$^+$X$^-$ membranes were also prepared via UV-photopolymerization using a protic ionic liquid version derived from TAA, TAAH$^+$MsO$^-$, as crosslinker. Some selected protic ionic liquid monomers were mixed with the crosslinker (5 or 10 wt% with respect to the protic ionic liquid monomers) and Darocur 1173 photoinitiator (5 wt % with respect to the protic ionic liquid monomers), avoiding the use of extra solvent since the pre-polymeric mixture is liquid. The resulting mixture was then poured into a silicone mold and exposed to UV light for photopolymerization: samples were irradiated for 60 s using a UVC-5 (DYMAX) UV Curing Conveyor System with an intensity up to 400 mW cm^{-2}, 30 mm lamp-to-belt distance, and belt speed at 7 m min^{-1}. An additional cleaning step was carried out to remove unreacted protic ionic liquid monomers, by leaving the resulting photopolymerized membranes in water for 2 h. The purity of the final dried membranes was checked by FTIR.

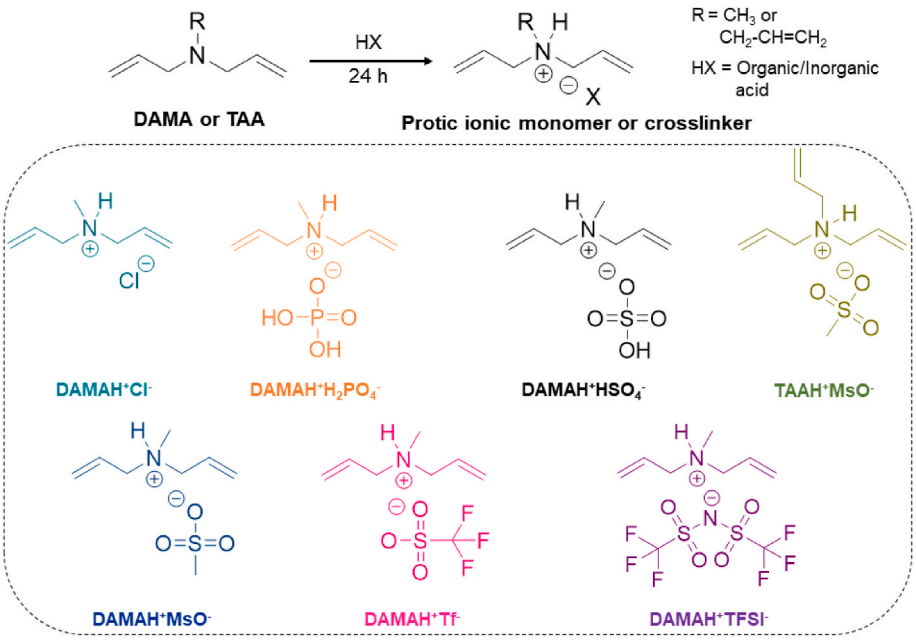

Scheme 1. Synthesis procedure and chemical structure of protic ionic liquid monomers DAMAH $^{+}$ X^{-}.

2.4. Characterization methods

^{1}H NMR spectra were recorded in a Bruker Avance DPX 300 at 300.16 MHz, using deuterated water (D_2O) or dimethylsulfoxide (DMSO) as solvents at room temperature. Protic ionic liquid monomers and their polymeric version were properly dissolved before the experiments. Fourier transform infrared (FTIR) spectra were measured for all protic monomers and their polymeric version on a Bruker Alpha II spectrophotometer employing Platinum ATR module with diamond window.

The thermal stability of the protic ionic liquid monomers and their corresponding protic polymers were investigated by thermogravimetric analysis (TGA) performed on a TGA Q500 from TA Instruments. The samples were heated at 10 °C min^{-1} under a N_2 atmosphere from room temperature to 800 °C. Differential scanning calorimetry was employed to detect the Tg of the protic poly(ionic liquids) by measurements on a DSC Q2000 from TA Instruments. The DSC scans were performed at heating and cooling rates of 10 °C min-1 from −60 °C to 200 °C. Dynamic Mechanical Analysis (DMA) was performed using a TA Instruments DMA Q800 apparatus. Scans were conducted from 0.01 to 35 Hz at 25 °C.

Electrochemical impedance spectroscopy (EIS) was employed to determine the ionic conductivity of the protic ionic liquids and their protic polymers in an Autolab 302 N potentiostat galvanostat at different temperatures (30–100 °C). An equilibration time of 20 min was required before every measurement. The samples were placed in between two stainless steel electrodes (surface area of 0.5 cm^2). Measurements were recorded in the 100 kHz to 1 Hz range, with 10 mV amplitude. Samples had an average thickness between 0.8 mm and 0.1 mm. When protic ionic liquid monomers were measured, the cell assembly was carried out inside a glovebox to avoid any humidity that may increase the ionic conductivity of the ionic liquids. Protic polymeric membranes were maintained in the oven at 60 °C during 48 h before every conductivity measurement.

2.4.1. Humidity uptake (%)

Humidity uptake of protic poly(ionic liquid)s was evaluated at room humidity as a function of time. Once dried in oven during 48 h at 60 °C (W_0), PEMs were exposed to a room humidity of 75.5% during *t* time and were weighted (W_t). This process was repeated until a constant weight was reached. The swelling percentage was calculated as follows:

$$\textit{Humidity uptake}\ (\%) = \frac{W_t - W_0}{W_0}\ x\ 100$$

Each point of the humidity uptake curve belongs to the average of three individual determinations.

2.4.2. Tensile strength test

For the tensile tests, protic poly(ionic liquid) membrane samples with bone shapes of 25 mm in length and cross-section 3.5 mm × 1 mm were used. Tests were carried out using a TA HD plus Texture Analyzer equipment (Texture Technologies) at 23 °C, 50% relative humidity, and an elongation rate of 25 mm min^{-1}. At least five tests were carried out for each sample.

2.4.3. Cyclic voltammetry (CV)

CV measurements were performed using a Bio-Logic Multi Potentiostat VMP3 in an Ar filled dry box. Protic ionic liquids (8 mM) were dissolved in a solution of 0.1 M $TBAPF_6$ in anhydrous ACN used as supporting electrolyte. Experiments were performed using a standard three-electrode electrochemistry system, which involved a platinum disk as the working electrode, a Pt wire as the counter electrode, and an Ag wire as the quasi-reference electrode. The Pt disk working electrode was polished using 0.3 μm alumina with subsequent ultrasonic cleaning for 30 s in ethanol. All data were recorded with a 0.1 V/s scanning rate at room temperature and monomers were dried under vacuum before analysis to avoid water traces.

2.4.4. Neutron scattering of protic P(DAMAH^{+}MsO^{-})

An aqueous dispersion of the thermally synthesized homopolymer P(DAMAH^{+}MsO^{-}) was produced by stirring solid polymer in water for 1 h. The aqueous dispersion (10 or 1 wt% for reflectivity and QENS studies, respectively) was then: i) casted on aluminum foil (QENS studies); ii) spin-coated onto Silicon blocks at 1800 rpm for 2 min (reflectivity studies). Films were completely dried in a vacuum oven at 60 °C for 48 h before measurements.

The polymer thermal stability was evaluated by determining the structural and dynamic response. Dynamical studies were performed on BASIS [33] spectrometer at SNS (US) using an Energy resolution (Eres) of 3.5 μeV; this specific configuration allows investigating relaxation

processes up to a few nanosecond timescale. Polymer samples of varying water/humidity uptake were loaded into thin-walled annular Al cans that were hermetically sealed with Indium wire; experiments were performed to follow the evolution of both elastic and quasielastic signal over a temperature scan (i.e., Elastic/Inelastic fixed window scans; EFWS/IFWS). Structural studies were performed at the Institut Laue Langevin (France) using the D17 reflectometer [34]. Polymer thin films (40–55 nm) were loaded in a sealed oven with humidity control provided by exposure to combined dry and hydrated gas flows to achieve desired temperature and humidity.

3. Results and discussion

3.1. Synthesis and characterization of protic ionic liquid monomers

First, new protic ionic liquid monomers were synthesized according to Scheme 1 by direct neutralization of the base diallylmethylamine (DAMA) and different organic or inorganic acids. Since the neutralization is an exothermic process, an ice bath was used during proton exchange reaction. As shown in Scheme 1, different protic ionic liquid monomers were synthesized by reacting equimolar amounts of base and acids leading to DAMAH$^+$ $H_2PO_4^-$, DAMAH$^+$Cl$^-$, DAMAH$^+$ HSO_4^-, DAMAH$^+$MsO$^-$, DAMAH$^+$Tf$^-$ and DAMAH$^+$TFSI$^-$. Furthermore, we synthesized one trifunctional allyl protic ionic liquid monomer based on triallylamine (TAA) to be used as an ionic crosslinker: TAAH$^+$MsO$^-$.

Ionic liquid properties like viscosity, hydrophilicity and ionic conductivity are strongly dependent of the anion type [35]. Normally, the decrease of viscosity means an increase of ionic conductivity. All the protic ionic liquid monomers show a homogeneous liquid appearance with an increasing apparent viscosity governed by the anion in the order TFSI$^-$ < Tf$^-$ < MsO$^-$ < HSO_4^- < $H_2PO_4^-$ < Cl$^-$. As an exception, DAMAH$^+$Cl$^-$ formed a solid protic ionic salt, with a melting point temperature at 65 °C, instead of a liquid which may be due to the strong ionic interaction between the cation and chorine Cl$^-$. The same trend observed for protic ionic liquids apparent viscosity was detected with respect to hydrophilicity: DAMAH$^+$TFSI$^-$ is a hydrophobic monomer (commonly observed for fluorinated compounds) while DAMAH$^+$Cl$^-$ is a strong hydrophilic monomer. Viscosity, hydrophilicity and ionic conductivity are governed by electrostatic interactions and charge delocalization. Cl$^-$ protic ionic liquid presents a strong H-bonding but a poor charge delocalization, which makes it a solid ionic liquid at room temperature and the most hydrophilyc monomer among the others, while HSO_4^- and $H_2PO_4^-$ protic monomers present a better charge delocalization than the chloride one but still a good hydrogen bonding, following the viscocity and hydrophilicity tendency. Following the trend, mesylate and triflate monomers are protic ionic liquids able to delocalize better the charge than the inorganic anions due to the S═O group, being Tf$^-$ a fluorinated anion that decreases the polarizability of the group. Finally, TFSI$^-$, a hydrophobic protic ionic liquid monomer due to its highly electronegative group.

The chemical structure of the corresponding protic ionic liquid monomers was first corroborated by ^{1}H NMR in DMSO. Fig. S1 presents the spectra of DAMA, the base, H_2SO_4, the acid, and DAMAH$^+$ HSO_4^-, the formed protic monomer. This last one presents all base and acid signals with the corresponding shifting of the labile cationic proton, confirming the formation of the ionic liquid. DAMAH$^+$TFSI$^-$ spectrum is shown in Fig. 1, as an example for peak assignment, where H_e singlet at 2.75 ppm chemical shift belongs to N^+-CH_3, H_d multiplet between 3.5 and 4 ppm corresponds to N^+-CH_2- hydrogens, $H_{b\text{-}c}$ multiplets represent the characteristics vinylic signals (5.5 and 6 ppm) CH═CH_2 and H_a singlet belongs to NH$^+$ proton chemical shift at 9.7 ppm. The presence of the NH$^+$ proton and proper integration of all peaks confirmed the successful protic ionic liquid monomer formation. All integration peaks of ^{1}H NMR spectra can be observed for the seven protic ionic liquid monomers in Figs. S2–8, confirming the stoichiometric formation of each protic compound, following the peak assignation of Fig. 1. The labile proton associated to the ammonium cations appear between 8.5 and 12 ppm as a singlet, and in the case of DAMAH$^+$ $H_2PO_4^-$ and DAMAH$^+$ HSO_4^-, the corresponding integration peak represents three or two protons depending on the extra hydrogens in the anionic structure. Fig. S9a presents the peak assignation of DAMAH$^+$MsO$^-$ spectrum, as an example of the methylated anionic protic monomer. As observed, a good integration and peak assignment was carried out indicating a high level of purity.

The new protic ionic liquids chemical structures were also confirmed by FTIR as shown in Fig. 1b and S9b. The appearance of a broad band at frequencies between 3000 and 2500 cm^{-1} evidences the presence of the ammonium group by the successful formation of the proton transferred salts. All spectra present an absorption band at around 1470 cm^{-1}, characteristic of N^+-CH_3 bending vibration from the pendant methyl units of the polycation backbone. Other characteristics bands are the ones present in sulfonic or sulfone anions, like DAMAH$^+$ HSO_4^-, DAMAH$^+$MsO$^-$, DAMAH$^+$Tf$^-$, and DAMAH$^+$TFSI$^-$ protic ionic liquid based spectra, which present S═O strong asymmetric vibration absorption bands between 1270 and 1170 cm^{-1}. S–C stretching vibration peak appears for MsO$^-$ (strong), Tf$^-$ (weak) and TFSI$^-$ (weak) at 770 cm^{-1}. C–F_3 asymmetric bending peak appears at 576 cm^{-1} for the trifluoromethane anions, and a doublet TFSI$^-$ molecular vibration band is observed in the region of 700–800 cm^{-1} due to the hydrogen interaction N–H–N between DAMA and the anion [36]. At 1100 cm^{-1} a broad band

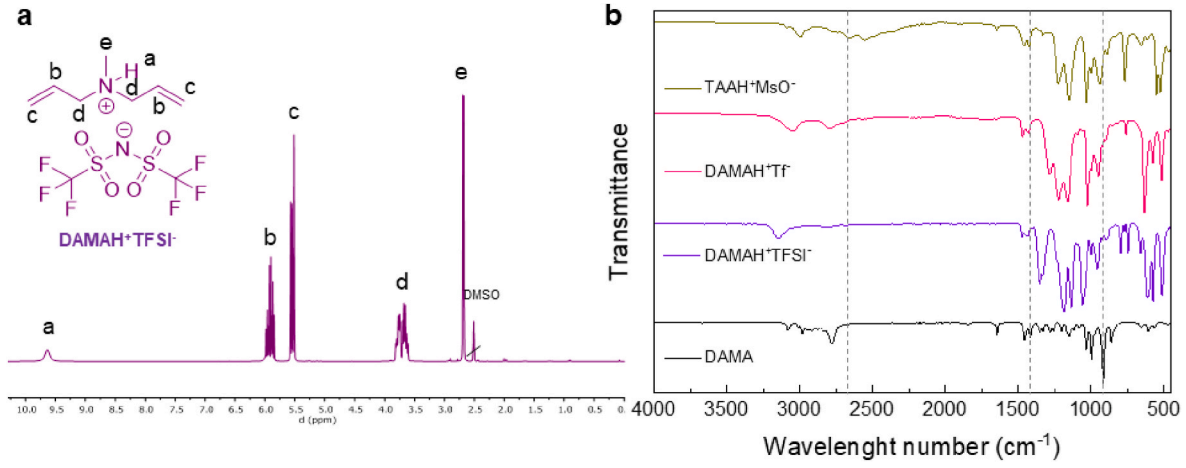

Fig. 1. ^{1}H NMR spectra of DAMAH$^+$TFSI$^-$ in DMSO-d_6 (a) and FTIR spectra of some polymerizable protic ionic liquids compared to the amine base DAMA employed for their synthesis (b).

appears due to PO_4 presence in DAMAH$^+$ $H_2PO_4^-$ structure. DAMA most important bands are also present in the protic ionic liquid monomer spectra at 1400 cm^{-1} and 1000-900 cm^{-1} regions that belong to the double bond monosubstituted bending absorption peaks.

Ionic conductivities of all the DAMA protic ionic liquid monomers are shown in Fig. 2a. At 100 °C, DAMAH$^+$TFSI$^-$ presented the highest ionic conductivity of 1.6 × 10^{-2} S cm^{-1} while the lowest 8 × 10^{-4} S cm^{-1} was achieved by DAMAH$^+$ $H_2PO_4^-$. The ionic conductivity trend matches with the aforementioned viscosity and hydrophilicity of the synthesized protic ionic liquid monomers and it is also related to the ΔpKa value of the acid, in which when viscosity decreases and ΔpKa increases, the ionic conductivity increases [37]. Thus HTFSI is the strongest acid and leads to protic ionic liquids with higher ionicity, the lowest hydrophilicity and lowest viscosity of the formed protic ionic liquid; while H_3PO_4 is the weakest acid and presents the lowest ionic conductivity; both of them present similar, but yet higher, conductivities than their non-polymerizable imidazolium protic verison, where TFSI$^-$ protic ionic liquid presents a value around 6 × 10^{-3} S cm^{-1} and the phosphate one shows an ionic conductivity around 1 × 10^{-5} S cm^{-1} at 100 °C [18,31,38]. The triflate protic, DAMAH$^+$Tf$^-$ is the second protic ionic liquid of highest ionic conductivity around 1.2 × 10^{-2} S cm^{-1} at 100 °C on dry conditions, an expected behavior since it is known that protic ionic liquids with fluorinated anions present high ionic conductivity [39]. Mesylate protic ionic liquid shows a slightly lower conductivity, around 9.7 × 10^{-3} S cm^{-1}. Sulfonated protic ionic liquid monomers present similar ionic conductivities than their triethylammonium or triethanolammonium non-polymerizable protic ionic liquid versions reported in the literature [24,25,31]. However, DAMAH$^+$$HSO_4^-$, DAMAH$^+Cl^-$ and in particular DAMAH$^+$ $H_2PO_4^-$ present much lower ionic conductivity at 100 °C than the fluorinated ones, following the viscocity and hydrophilicity trend mentioned before, goberned by the electrostatic interactions between the protic cation and the anion, and the charge delocalization. Finally, regarding the cationic contribution of the ionic conductivity performance, it has been reported that protic ionic liquids possessing allylammonium cations exhibit higher conductivities than the corresponding alkyl cation ones [40]. In general, these results are in agreement with the ionic conductivity data of the literature in other types of protic ionic liquids [23,24].

Cyclic voltammetry (CV) was performed to investigate the proton activity of DAMAH$^+$MsO$^-$ and DAMAH$^+$Tf$^-$ as examples. As shown in Fig. 2b, the CV curve of both protic ionic liquid monomers presented the characteristics reduction and oxidation peaks of protons: the negative peak at around −1 V vs Ag/Ag^{+1} is assigned to the reduction reaction of the labile H^+ to H_2, and the anodic peak at −0.4 V and −0.1 V vs Ag/Ag^{+1} for DAMAH$^+$ Tf$^-$ and DAMAH$^+$MsO$^-$, respectively can be assigned to the hydrogen oxidation reaction (HOR). Considering that both protic ionic liquids have the same amount of dissociable protons in the cation, the triflate one shows higher reduction current and a more reversible redox process. The electrochemical behavior confirmed that the labile H^+ on both protic ionic liquid monomers are active and thus, they are of great potential for the synthesis of membranes for fuel cell applications.

Thermal stability of all protic DAMA monomers are shown in Fig. S10. It can be observed that, for the majority of the protic monomers, the T_d (temperature at a weight loss of 5%) below 200 °C that can be attributed to the removal of residual moisture adsorbed from the air during the experiment. This observation agrees with the hydrophilicity trend since the triflate and TFSI$^-$ protic based monomers present the T_d at much higher temperatures due to the presence of fluorinated anions [35,39]. In particular, DAMAH$^+$Tf$^-$ and DAMAH$^+$TFSI$^-$ present good thermal stability with degradation temperatures higher than 250 °C.

3.2. Polymerization of DAMAH$^+$ X^- protic ionic liquid monomers

3.2.1. Thermal free radical polymerization

Diallylammonium monomers such as diallyldimethylammonium chloride are known to polymerize using radical initiators through a cyclopolymerization mechanism [41–44]. Mechanisms and polymerization conditions for similar diallylmethylamines and its protonated and quaternary forms were studied before by Timofeeva et al. [45]. From the seven protic monomers synthesized here, DAMAH$^+$Cl$^-$ was discarded due to its high hydrophilicity regarding the future potential application, while DAMAH$^+$ $H_2PO_4^-$ was discarded due to its low ionic conductivity. Finally, the mesylate trifunctional monomer was unwanted for thermal polymerization because its only use was as a crosslinker. Thus, polymerization of the protic ionic liquid monomers DAMAH$^+$ HSO_4^-, DAMAH$^+$MsO$^-$, DAMAH$^+$Tf$^-$, and DAMAH$^+$TFSI$^-$ was carried out using free radical initiators. The scheme at Fig. 3 represents as an example the thermal polymerization process employing DAMAH$^+$MsO$^-$. A similar procedure was carried out for the hydrophilic monomer DAMAH$^+$ HSO_4^-. In these cases, monomers were polymerized in high yields (95% for DAMAH$^+$MsO$^-$ and 91% for DAMAH$^+$ HSO_4) in water as solvent at 70 °C employing a water soluble diazo thermal initiator (AIBA). However, for the fluorinated monomers such as DAMAH$^+$Tf$^-$ or DAMAH$^+$TFSI$^-$ the polymerization yield was very low (19 and 21% respectively) and their use to explore this polymerization technique was left-over. After purification, the protic poly(ionic liquid)s were casted on silicon molds to obtain a homogeneous and transparent self-standing PEM of around 400 μm thickness, as observed in scheme. P(DAMAH$^+$MsO$^-$) was obtained as a flexible but self-standing membrane while P(DAMAH$^+$ HSO_4^-) was a harder and brittle membrane.

Fig. 3 shows the ^{1}H NMR spectrum in D_2O of P(DAMAH$^+$MsO$^-$) which confirms the typical cyclopolymerization mechanism of diallylammonium monomers [42,43]. The spectrum shows that the

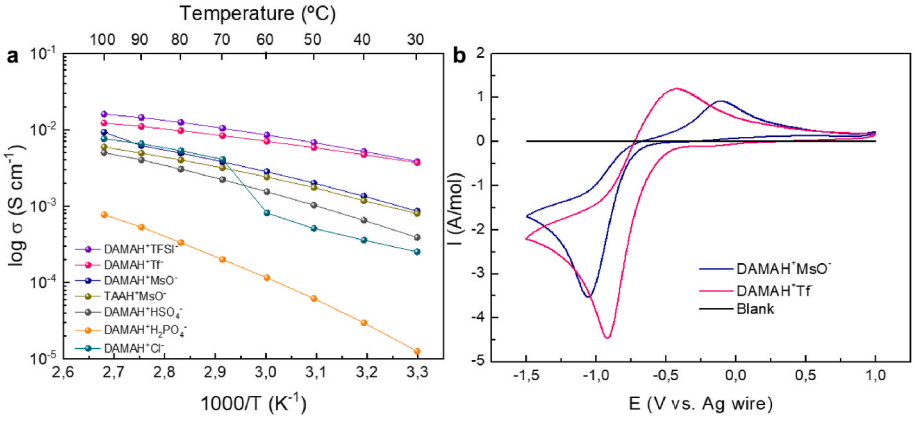

Fig. 2. Ionic conductivity determined by EIS of all synthesized protic ionic liquid monomers and crosslinker (a) and cyclic voltammetry measurements (CVs) of 8 mmol of DAMAH$^+$MsO$^-$ and 8 mmol of DAMAH$^+$Tf$^-$ in 0.1 M $TBAPF_6$/ACN solution (b).

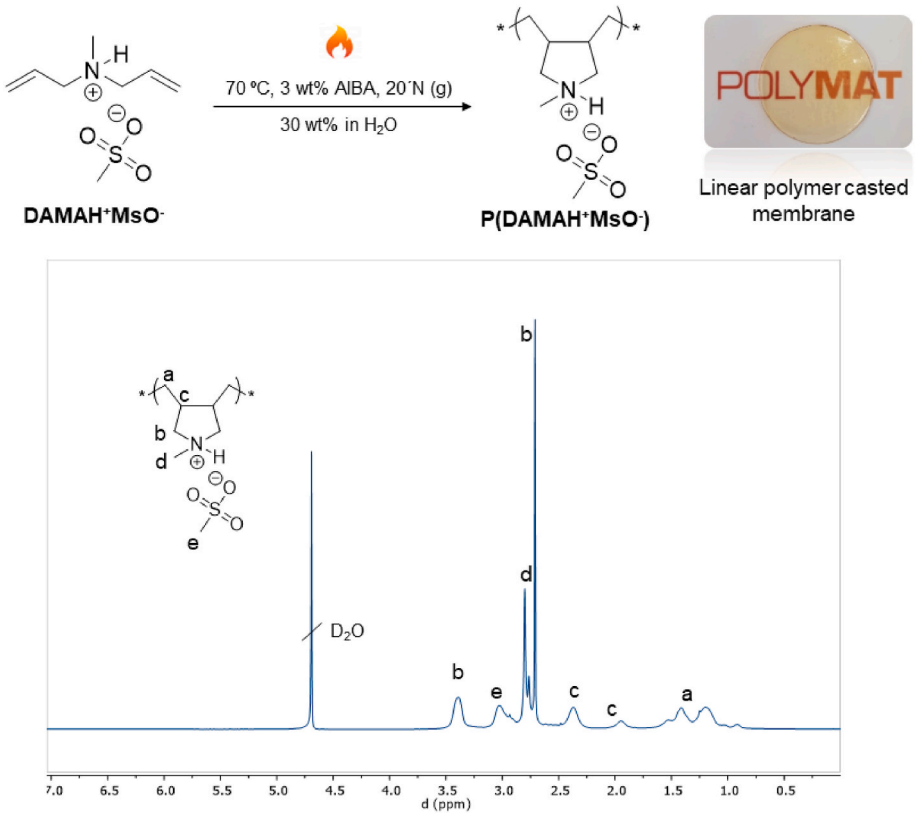

Fig. 3. Free-radical cyclopolymerization of diallylammonium mesylate $DAMAH^+MsO^-$ and ^1H NMR spectrum of $P(DAMAH^+MsO^-)$ in D_2O.

unreacted monomers (aprox. 5 wt%) were completely removed after the dialysis purification process. The associated signals with vinylic protons between 5.5 and 6.0 ppm (see Figs. S2–9, ^1H NMR spectra of the prepared protic ionic liquid monomers) disappeared after the thermal polymerization reaction, showing that the monomer complete conversion was accomplished. Furthermore, the characteristic chemical shifts arising from the cyclic pyrrolidinium backbone can be clearly observed ($H_{a\text{-}d}$ of the spectrum) along with the methylic hydrogens from the mesylate anion (H_e at 3 ppm).

FTIR was carried out to corroborate not only the disappearance of the vinylic absorption peaks of the monomers, but also to identify the characteristics bands of the protic poly(diallylammonium) materials. Fig. S11a shows that all main protic ionic liquid peaks are present and that those that correspond to the C=C groups disappear after the polymerization: 1400 and 1000-900 cm^{-1}, confirming again the successful polymerization process. The N^+-CH_3 bending vibration at around 1470 cm^{-1} and the S=O strong asymmetric vibration absorption band between 1270 and 1170 cm^{-1} are present, demonstrating that the polycation and anions from $P(DAMAH^+HSO_4^-)$ and $P(DAMAH^+MsO^-)$ were not affected by the polymerization procedure. Thermal stability is a key parameter that determines the application and temperature range of the obtained membranes. TGA analysis is shown in Fig. S11b, in which a T_d was shown for values above 200 °C for both protic polymeric membranes, a high degradation temperature. Considering T_d, $P(DAMAH^+MsO^-)$ presents higher thermal stability than $P(DAMAH^+HSO_4^-)$, where the first protic polymer starts to degrade with a 5 wt% at 300 °C and the sulfonate one does it at 250 °C. At the end of the last section (3.2.3 Characterization of membranes) thermal stability and hydration reversibility of $P(DAMAH^+MsO^-)$ via neutron experiments were carried out in order to guarantee the potential application of this material as PEMFCs.

3.2.2. *Photoinitiated free radical polymerization of $DAMAH^+X^-$ based protic ionic liquid monomers*

It is well known that diallylammonium monomers can be photopolymerized using radical photonitiators under a similar mechanism leading to polymer membranes or coatings [47]. Photopolymerization is also considered as a fast and versatile method to obtain membranes for energy applications [48]. Thus, we investigated the photopolymerization of some protic ionic liquid monomers. $DAMAH^+MsO^-$, $DAMAH^+Tf^-$ and $DAMAH^+TFSI^-$ liquid monomers (chosen among all synthesized protic monomers due to their better thermal and conductivity properties, compared on section 3.1) were mixed with 5 wt% of Darocur as photoinitiator and with 5 or 10 wt% of the trifunctional monomer $TAAH^+MsO^-$ as crosslinker. Once the photopolymerization was carried out, the crosslinked membranes were purified in Milli Q water during 2 h in order to eliminate unreacted monomers or initiator. Scheme 2 shows an example of the photo co-polymerization process of a monomer mixture of $DAMAH^+Tf^-$ and $DAMAH^+MsO^-$.

Photopolymerization allows to obtain crosslinked homopolymers in a simple process. It is worth to mention that this easy polymerization process allowed to mix diverse protic ionic liquid monomers with the intention of combining their different properties in a cross-linked random copolymer. Following Scheme 2, relatively thin membranes (between 100 and 250 μm) were prepared through photopolymerization of different homopolymers such as $P(DAMAH^+MsO^-)$ and $P(DAMAH^+TFSI^-)$ or copolymers with different composition ratios $P(DAMAH^+MsO^-_{70}/TFSI^-_{30})$, $P(DAMAH^+MsO^-_{50}/TFSI^-_{50})$ and $P(DAMAH^+MsO^-_{50}/Tf^-_{50})$. The protic copolymer compositions were chosen with the intention of seeing an effect on the protic polymer properties when hydrophilic (mesylate) and hydrophobic ($TFSI^-$) protic monomers are employed. $P(DAMAH^+MsO^-_{50}/Tf^-_{50})$ was also sinthesized in order to prepare and characterize a protic copolymer based on hydrophilic monomers with one of them fluorinated. After the photopolymerization, membranes could be easily handled and showed good apparent mechanical properties. Membranes with only 5 wt% of protic crosslinker

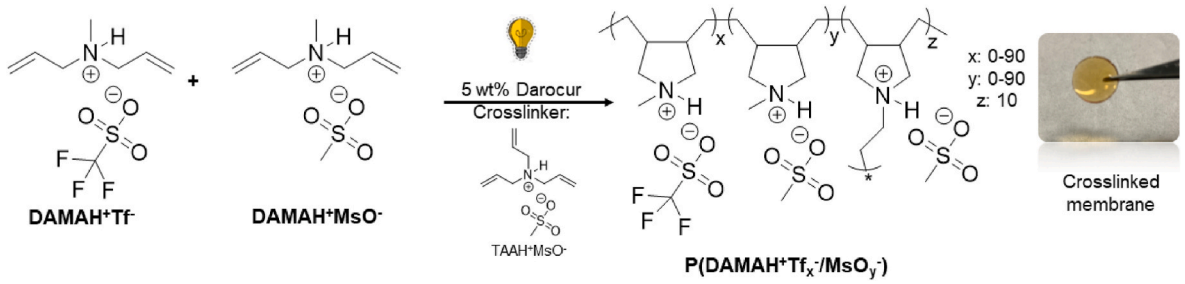

Scheme 2. Photo co-polymerization process of diallylmethylammonium monomers $DAMAH^+Tf^-$ and $DAMAH^+MsO^-$.

were also synthesized but the manageability of the membranes was not good enough since they were too soft (the apparent mechanical properties were lower than employing 10 wt% of crosslinker in the protic polymers).

Fig. 4a shows the FTIR spectra and thermal stability of the materials. The FTIR spectra show the almost absence of the vinylic absorbance peaks at 1400 and 900 cm^{-1} indicating that the polymerization was quantitative and the presence of the characteristic peaks of the different anions in the region of 1270-600 cm^{-1}. Again, the characteristic peak of the polydiallylmethylammonium, N^+-CH_3, was still present at 1470 cm^{-1} and sulfonic and sulfone bands between 800 and 500 cm^{-1} are present in the spectrum, like S–C stretching vibration peak at 770 cm^{-1}, C–F_3 asymmetric bending peak at 576 cm^{-1} for the trifluoromethane anions, and a particular doublet $TFSI^-$ molecular vibration band in the region of 700–800 cm^{-1} due to the hydrogen interaction N–H–N named before. TGA curves (Fig. 4b) demonstrate the good thermal properties of the materials, where a T_d 5 wt% weight loss was observed between 200 and 300 °C, considering also the moisture lost during the experiment. Even if all of them present a quite proper thermal stability, the anion involved in the polymer governs this important property. Polydiallylmethylammonium $TFSI^-$ based materials are more thermally stable and exhibit a 5 wt% weight loss at higher temperatures than the polymers based on MsO^- or Tf^-.

3.2.3. *Characterization of protic P(DAMAH$^+X^-$) membranes*

Next, obtained membranes by thermal and photopolymerization with different compositions were characterized in terms of mechanical, humidity uptake and ionic conductivity properties. Dynamic mechanical, tensile and humidity uptake tests were carried out only for the most promising photocured protic materials.

Dynamic mechanical analysis (DMA) was carried out in order to, first of all, give an idea of the storage modulus (E') that the polymeric membranes present, synthesized in this work for the first time with no adition of extra plastizasers, ILs, among others; and also to compare E' when different anions were involved in the protic poly(ionic liquid) membranes (Fig. 5a). High E' modulus results were observed for the analyzed membranes with values between 10^7 and 10^5 Pa, values considered as high taking into account that Nafion 212 presents storage modulus around 10^8 Pa at the same conditions [46]. It is clearly observed the contribution of the different anions to E' at 1 Hz frequency and 25 °C: when MsO^- protic poly(ionic liquid) is synthesized, the storage modulus is 6.6×10^5 Pa, and when fluorinated anions intervene, E' modulus decreases to 4×10^5 Pa (for 30 wt% $TFSI^-$) and increases to 9×10^6 Pa (for 50 wt% Tf^-). In all cases, storage modulus (E') and loss modulus (E'') values were not only independent of frequency but also the values obtained for E' were higher than E'' for all membranes, confirming that the materials are crosslinked protic poly(ionic liquids). As a reference point, and due to the lack of mechanical properties studies of neat protic polymers, membranes based on non-protic PDADMA TFSI mixed with protic ionic liquids (HMIM $TFSI^-$ or Tf^-) in a 75:25 wt ratio present storage modules between 10^7 and 10^8 Pa at 25 °C. This module values are one order of magnitude higher than the protic polymers presented in this work, meaning that these last ones, with no additives, are quite proper and can compete with the cited work published by Huang et al. [31]. In terms of anion contribution effect, it can be clearly observed the negative charge nature effect from the anion on the mechanical performance. MsO^- and Tf^- are sulfonate anions while $TFSI^-$ is a sulfonamide anion that may not strongly interact with MsO^- like Tf^- does. Finally, it has also been observed that Tf^- interacts preferably with protic ammonium cations than $TFSI^-$, other possible explication of the higher storage modulus of the protic co-polymer based on MsO^- and Tf^- anions than the sulfonamide anion [31].

Tensile tests were carried out in order to evaluate the strain capacity and to compare the effect of its composition. As observed in Fig. S12, between 25 and 30% strain was achieved for all polymeric protic ionic liquids: while for P($DAMAH^+MsO^-$) 10% $TAAH^+MsO^-$ a stress of 0.07 MPa was needed to break the membrane, only 0.04 MPa stress was required to break a membrane with 50 wt% of P($DAMAH^+TFSI^-$) for the same strain. When $TFSI^-$ or Tf^- were copolymerized with MsO^- the applied stress for breaking the membranes were in the middle of the homopolymers materials, following the trend. It is important to mention that Nafion 212, at the same conditions (dry state and 25 °C), normally

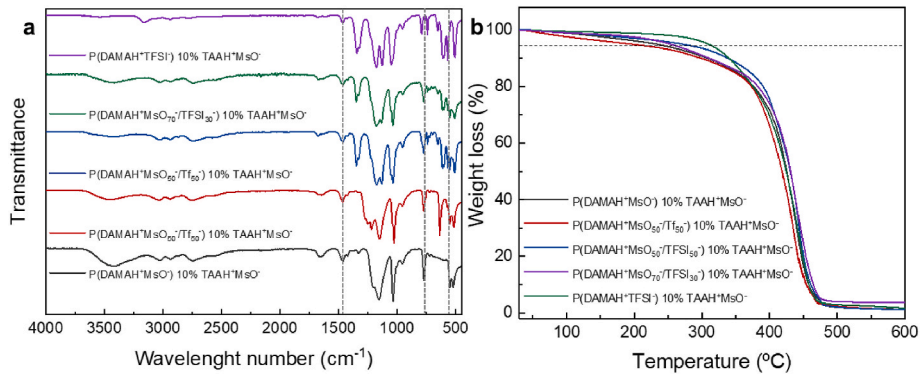

Fig. 4. FTIR spectra (a) and TGA results (b) of thin protic membranes crosslinked with 10% of $TAAH^+MsO^-$crosslinker.

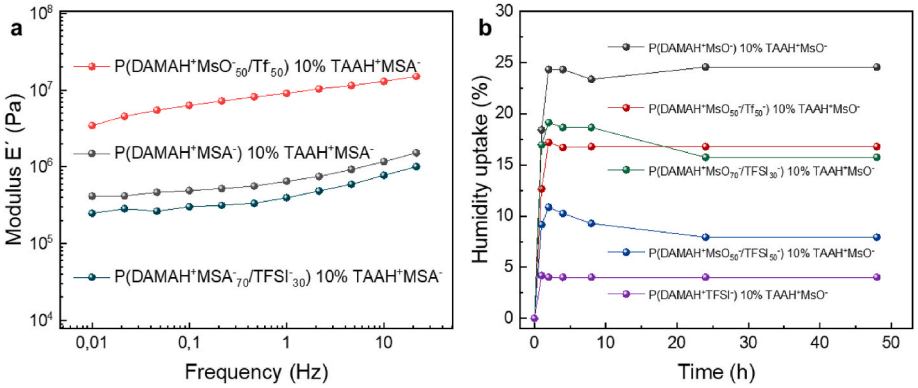

Fig. 5. Dynamic mechanical analysis (a) and humidity uptake of protic poly(diallyl ammonium) membranes obtained by photopolymerization (b).

presents three orders of magnitud higher (15 MPa aprox.) than the results obtained for these protic membranes.

The humidity uptake of the membranes was also evaluated since it is an important aspect for the development of PEMs due to its effect in the membrane mechanical stability and ionic conductivity. As observed in Fig. 5b, the membrane composition and, in particular the anion, shows a strong effect. The moisture uptake clearly depends on the content of the $TFSI^-$, a hydrophobic anion due to the highly electronegative trifluoromethylsulfonyl group. Thus, P(DAMAH$^+$ $MsO^-_{70}/TFSI^-_{30}$) 24 h exposed to 75.5% humidity absorbs less than 10% of weight, while the homopolymer P($DAMAH^+MsO^-$) absorbs 25% of its weight. All of them reach their equilibrium humidity uptake between 2 and 4 h of exposure. Interestingly, the copolymers show an intermediate behaviour. The fluorinated anion, Tf^-, also contributes decreasing the hydrophilicity with a less marked effect than $TFSI^-$.

The ionic conductivities of the polymers were determined by impedance spectroscopy (EIS) from 30 to 100 °C in the dry membranes. Fig. 6a presents the ionic conductivity of P(DAMAH$^+$ HSO_4^-) and P($DAMAH^+MsO^-$) obtained by thermal radical polymerization. A typical Arrhenius increase of the ionic conductivity with the temperature is observed. As expected, the protic polymer versions present a lower ionic conductivity, following the trend observed in Fig. 2a, than the protic monomers and, as expected, a hard membrane (P(DAMAH$^+$ HSO_4^-)) will present a lower conductivity (6.7×10^{-5} S cm^{-1} at 100 °C) than a soft and flexible one such as P($DAMAH^+MsO^-$) 5.1×10^{-4} S cm^{-1} at 100 °C. Interestingly, the lowest conductivities observed in Fig. 6a belong to the thermally polymerized membranes which may be due to its higher thickness.

As mentioned before, Fig. 6a presents also the ionic conductivity of the dry membranes obtained by photopolymerization, all of them presented superior conductivity than the ones thermally synthesized, with higher values than 1×10^{-3} S cm^{-1} at 100 °C. These results are in agreement also with the effect of the anion trend observed in the protic ionic liquid monomers. At 100 °C, P($DAMAH^+MsO^-$) homopolymer, P(DAMAH$^+$ $MsO^-_{50}/TFSI^-_{50}$), and P(DAMAH$^+$ MsO^-_{50}/Tf^-_{50}) showed an ionic conductivity of around 1.2×10^{-3} S cm^{-1} while P(DAMAH$^+$ $MsO^-_{70}/TFSI^-_{30}$) presented a slightly higher value of 2.2×10^{-3} S cm^{-1}. Considering the anhydrous condition of the experiment and the absence of any other compound that may help to increase the conductivity, these mobility values are surprisingly good. It is worth to remark that the polydiallylmethylammonium membranes presented a high ionic conductivity without the presence of any extra low molecular weight molecule like water, ionic liquids or acids. Neat non-protic version of the polymer, PDADMA, having $TFSI^-$ or Tf^- as anions, present low ionic conductivities around 10^{-6} for the first one and 10^{-9} S cm^{-1}for the triflic ionic polymer at 100 °C, lower ionic conductivities than the protic version presented in this work, showing the clear protic effect on the ammonium polymer [31]. On the other hand, other neat non-ammonium protic polymers present ionic conductivities between 10^{-4} and 10^{-7} S cm^{-1} at high temperatures [28,29,49,50], and Nafion 212, at low humidity (below 5%), conductivities of 10^{-9} to 10^{-5} S cm^{-1} have been reported [51].

Based on the obtained results, ionic conductivity measurements were made by varying the relative humidity (RH) at 80 °C to compare the behaviour of P($DAMAH^+MsO^-$) 10% $TAAH^+MsO^-$ and Nafion 212 reference membrane. Photocured P($DAMAH^+MsO^-$) was chosen due to the observed mechanical and tensile, humidity uptake and ionic conductivity properties. When compared, P(DAMAH$^+$ MsO^-_{50}/Tf^-_{50}) was

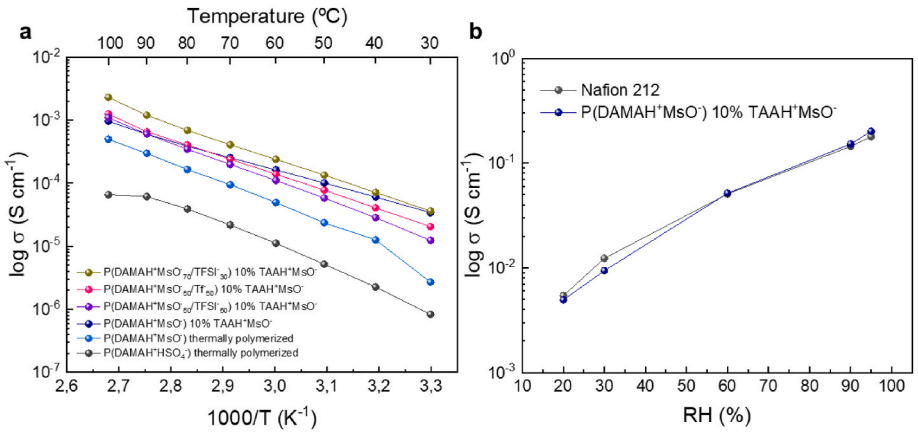

Fig. 6. (a) Ionic conductivity measured from 30 to 100 °C of all best and dried protic thermally and photo-crosslinked membranes; (b) ionic in plane-conductivity of photocured P($DAMAH^+MsO^-$) and Nafion 212 measured at 80 °C with variable relative humidity (RH) from 20 to 100% employing a climatic chamber to control both temperature and RH.

also a suitable candidate as it exhibits humidity uptake (a necessary characteristic for comparation with Nafion), but the idea was to further compare with a non-fluorinated protic polymer. As appreciated in Fig. 6b the ionic conductivity is similar as the one obtained when the fluorinated commercial membrane is employed. This is an indication that the conductivity properties of the developed protic poly(ionic liquid)s are exceptional with the potential advantage that at higher temperatures the protic synthesized materials may not need hydration to keep the high ionic conductivity values. Is also important to remark that the photocure protic polymer was compared specifically with Nafion 212 because this one is commonly used as membranes in fuel cells.

Next, ionic conductivity was measured for the best membranes at intermediate temperatures in anhydrous conditions from 70 to 120 °C. Photocured P(DAMAH$^+$MsO$^-$) and P(DAMAH $^+$ MsO$^-_{50}$/Tf$^-_{50}$) were chosen due to their mechanical and ionic conductivity properties compared to the other protic materials, while P(DAMAH$^+$TFSI$^-$) was chosen due to its high hydrophobicity and ionic conductivity. As observed in Fig. 7, protic polymeric materials showed high ionic conductivity with an increasing trend for higher temperatures. P(DAMAH$^+$MsO$^-$) presented a conductivity of 1.9×10^{-3} S cm^{-1}, a close value to P(DAMAH$^+$TFSI$^-$) (1.8×10^{-3} S cm^{-1}). When P(DAMAH $^+$ MsO$^-_{50}$/Tf$^-_{50}$) was evaluated, a slightly higher ionic conductivity was obtained: 2.1×10^{-3} S cm^{-1}. This highlights that these protic polymeric membranes employing MsO$^-$, TFSI$^-$ or Tf$^-$ anions showed very high ionic conductivities at intermediate temperatures.

Finally, thermal stability and hydration reversibility of the thermally polymerized P(DAMAH$^+$MsO$^-$) were evaluated via neutron experiments following two approaches: i) investigating intrinsic dynamics (Fig. 8a–b), and ii) studying membrane thickness and water uptake evolution (Fig. 8c–d). Thermally polymerized P(DAMAH$^+$MsO$^-$) was chosen for these experiments due to its high solubility and easy casting process, in comparation to the non-soluble chemically crosslinked protic polymers. Polymer dynamics were studied by following the scattering signal upon ramping the temperature up to 100 °C in dry (Fig. 8b; black symbols) and hydrated protic polymers (Fig. 8b; light to dark blue symbols - 5, 23 and 32 wt%). Complementary sample stability was ensured by the complete overlap of profiles after cooling (inset Fig. 8b). When increasing the temperature, protons-containing species become mobile; this causes a loss in elastic intensity associated with the appearance of QENS broadening. It is, therefore, possible to disentangle processes by following the evolution of the scattering signal by scanning the temperature, and more specifically, by evaluating slope shifts in the EFWS.

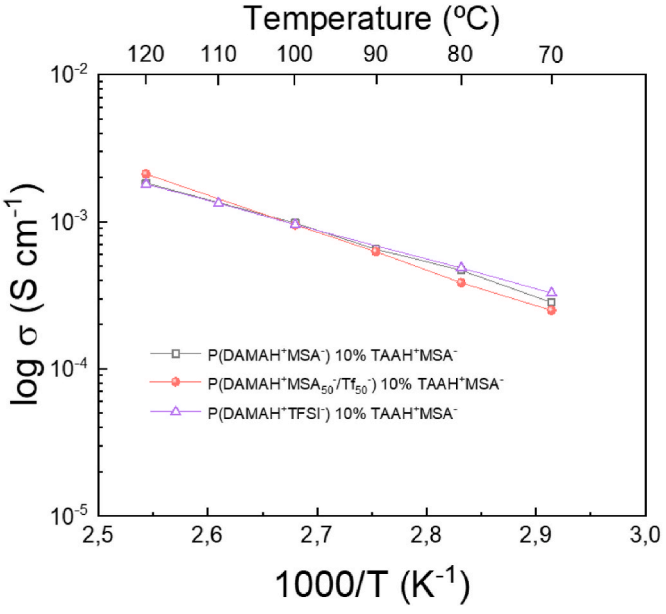

Fig. 7. Ionic conductivity measurement through EIS of P(DAMAH$^+$MsO$^-$), P(DAMAH $^+$ MsO$^-_{50}$/Tf$^-_{50}$), and P(DAMAH$^+$TFSI$^-$) membranes.

As shown in Fig. 8b, the initial loss of elastic intensity, accompanied with an increase in mean square displacement ($d\langle u^2\rangle/dt = 6.8 \pm 0.5$ 10^{-4} Å^2 K^{-1}), is associated with the activation of –CH$_3$ rotation at low temperature (~−220 °C) [52]. Increasing the temperature gets activated the polymer side chain relaxation (~−125 °C), followed by water dynamics (~−20 °C), which is mostly visible by the extremely pronounced change in slope in the hydrated sample (32 wt%; dark blue symbols; Fig. 8b). The level of hydration, as expected, affects water dynamics; we were, therefore, able to disentangle nanoconfined *vs* bulk-like dynamics by testing different samples. More specifically, nanoconfined dynamics ($E_A = 10.1 \pm 0.4$ kJ mol^{-1}) are visible when the polymer is hydrated at 5 or 23 wt% as suggested by the Q-independency of the IFWS; bulk-like dynamics ($E_A = 23.4 \pm 0.6$ kJ mol^{-1}) are visible when the polymer is fully hydrated (IFWS is Q-dependent). These values are comparable with results previously found for a different membrane [53].

Finally, dynamics are associated with the ion (localised) dynamics, which appears in the spectroscopic window as remaining intensity at high temperature for the dry polymer (>50 °C; mauve shaded area in Fig. 8b). The analysis of both side chain and ion dynamics suggest a strong coupling between these two processes, when examined in the nanosecond time-window, as they seem to have similar activation energy (5.6 ± 0.5 kJ mol^{-1}).

Dynamical stability is confirmed by the structural stability, when the polymer is investigated in form of a thin film. Upon heating (≥60 °C) we found that the membrane shrinks (~25%; inset Fig. 8d). This is due to a loss in hydration water, which is, however, completely recovered upon cooling, suggesting that the inner structure and porosity is not affected by the heating treatment. It is clearly observed that the material retains its properties after temperature cycling up to 120 °C. It is worth noticing at this point, that due to instrumental limitations, for instance the difficulty of ensuring exact reading of relative humidity while testing the sample at high temperature is difficult to asses the amount of water loss. However, if we compare the thickness of the same membranes fully-*vs* partially-hydrated (32 *vs* ~ 10 wt%) at high temperature (42 *vs* 39 nm), it is reasonable to assume that a certain level of hydration is retained, as confirmed by the dynamical studies. Alltogether, these results suggest the feasibility of this chemistry to be used for intermediate and potentially high-T operations.

4. Conclusions

This article presents poly(diallylmethylammonium X$^-$) proton conducting membranes with high ionic conductivity. First, the synthesis and characterization of a new protic ionic liquid monomers family was carried out based on a diallylmethylammonium cation and a variety of anions. Then, protic diallylmethylammonium monomers were polymerized using free radical thermal and photopolymerization. The protic ionic liquid monomers were sucessfully polymerized through a cyclopolymerization mechanism. Polymer membranes were prepared and characterized showing that mechanical and hygroscopic behaviours can be modulated and adjusted by the choice of the protic monomers. Poly (diallylmethylammonium X$^-$) membranes with MsO$^-$ and TFSI$^-$ anions showed the highest ionic conductivity values and the best combination of mechanical and thermal stability properties. Photocured P(DAMAH$^+$MsO$^-$) shows similar ionic conductivity values than Nafion 212 under varying relative humidity conditions at 80 °C. Furthermore, it shows a high ionic conductivity value of 1.9×10^{-3} S cm^{-1} at 120 °C under dry conditions. These results make the protic poly(diallylmethylammonium X$^-$) membranes promising candidates as intermediate or high temperature PEMs for fuel cells without additives that may leach.

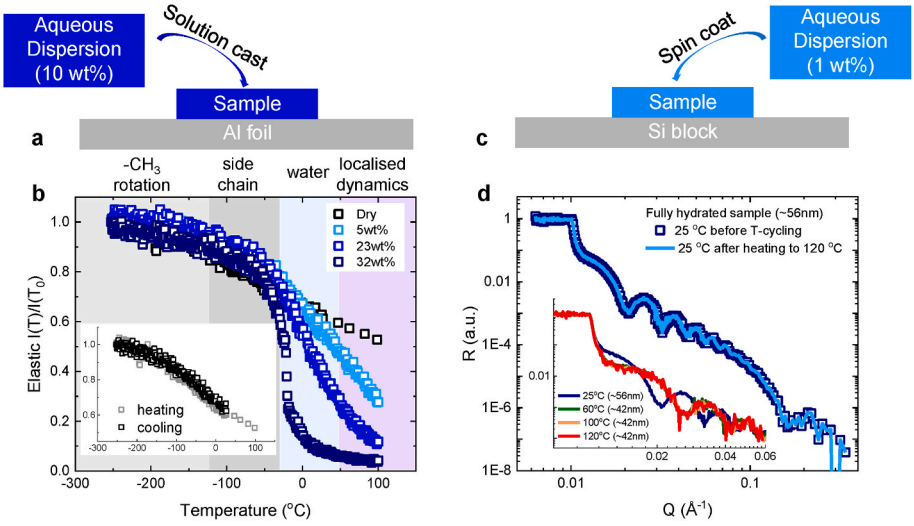

Fig. 8. (a) Cartoon explaining the sample preparing for QENS studies. (b) Elastic Fixed Window Scan (EFWS) as acquired on BASIS spectrometer by integrating scattering profiles at around 0 μeV Energy transfer. Data are presented for crumpled polymer at different level of hydrations: i) dry (vacuum oven treated for 48 h at 60 °C; black symbols); ii) 5 wt% H_2O-hydrated -low- (~10 min exposure at 40% relative humidity; light-blue symbols); iii) 23 wt% H_2O-hydrated -intermediate- (~2 h exposure at 40% relative humidity; blue symbols); vi) 32 wt% H_2O-hydrated -high- (~2 h exposure at 98% relative humidity; dark-blue symbols). The inset shows the reversibility of the test performed on the dry sample. (c) Cartoon explaining the sample preparing for Neutron Reflectivity studies. (d) Reflectivity profiles for thin-film deposited on silicon block; data are presented for highly hydrated samples at 25 °C before and after T-cycling (temperature cycling) (up to 120 °C). The inset shows the profiles during the T-cycling. (For interpretation of the references to colour in this figure legend, the reader is referred to the Web version of this article.)

Funding sources

The authors would like to thank the European Commission for financial support through funding from the European Union's Horizon 2020 research and innovation program under the Marie Sklodowska-Curie grant agreement No 823989 and Spanish AEI-MINEC for funding through project PID2020-119026 GB-I00. A portion of this research used resources at the Spallation Neutron Source, a DOE Office of Science User Facility operated by the Oak Ridge National Laboratory. Authors are grateful to ILL for neutron beamtime (https://doi.org/10.5291/ILL-DATA.9-11-2016). F.F. would like to acknowledge the EPSRC (grant EP/V057863/1) for funding.

Author information

The manuscript was written through contributions of all authors. All authors have given approval to the final version of the manuscript.

CRediT authorship contribution statement

Antonela Gallastegui: Conceptualization, Methodology, Validation, Investigation, Writing – original draft, Writing – review & editing, Visualization. **Fabrizia Foglia:** Investigation, Validation, Visualization, Writing – original draft. **Paul F. McMillan:** Supervision. **Nerea Casado:** Investigation, Writing – original draft. **Aurelie Gueguen:** Term, Conceptualization, Validation, Investigation, Funding acquisition. **David Mecerreyes:** Term, Conceptualization, Methodology, Writing – review & editing, Supervision.

Declaration of competing interest

The authors declare the following financial interests/personal relationships which may be considered as potential competing interests: David Mecerreyes reports financial support was provided by POLYMAT, University of the Basque Country.

Data availability

Data will be made available on request.

Acknowledgment

The authors thank for technical and human support provided by IZO-SGI SGIker of UPV/EHU. Technical and human support provided by IZO-SGI, SGIker (UPV/EHU, MICINN, GV/EJ, ERDF and ESF) is gratefully acknowledged for assistance.

Appendix A. Supplementary data

Supplementary data to this article can be found online at https://doi.org/10.1016/j.polymer.2023.126064.

References

[1] H. Zhang, P.K. Shen, Advances in the high performance polymer electrolyte membranes for fuel cells, Chem. Soc. Rev. 41 (2012) 2382–2394, https://doi.org/10.1039/C2CS15269J.

[2] R. Haider, Y. Wen, Z.F. Ma, D.P. Wilkinson, L. Zhang, X. Yuan, S. Song, J. Zhang, High temperature proton exchange membrane fuel cells: progress in advanced materials and key technologies, Chem. Soc. Rev. 50 (2021) 1138–1187, https://doi.org/10.1039/D0CS00296H.

[3] V.M. Ortiz-Martínez, A. Ortiz, V. Fernández-Stefanuto, E. Tojo, M. Colpaert, B. Améduri, I. Ortiz, Fuel cell electrolyte membranes based on copolymers of protic ionic liquid [HSO3-BVIm][TfO] with MMA and hPFSVE, Polymer 179 (2019), 121583, https://doi.org/10.1016/j.polymer.2019.121583.

[4] G. Venugopalan, K. Chang, J. Nijoka, S. Livingston, G.M. Geise, C.G. Arges, Stable and highly conductive polycation–polybenzimidazole membrane blends for intermediate temperature polymer electrolyte membrane fuel cells, ACS Appl. Energy Mater. 3 (2020) 573–585, https://doi.org/10.1021/acsaem.9b01802.

[5] C.S. Gittleman, H. Jia, E.S. De Castro, C.R. Chisholm, Y.S. Kim, Proton conductors for heavy-duty vehicle fuel cells, Joule 5 (2021) 1660–1670, https://doi.org/10.1016/j.joule.2021.05.016.

[6] X. Ge, F. Zhang, L. Wu, Z. Yang, T. Xu, Current challenges and perspectives of polymer electrolyte membranes, Macromolecules 55 (2022) 3773–3787, https://doi.org/10.1021/acs.macromol.1c02053.

[7] J. Walkowiak-Kulikowska, J. Wolska, H. Koroniak, Polymers application in proton exchange membranes for fuel cells (PEMFCs), Phys. Sci. Rev. 2 8 (2017), 20170018, https://doi.org/10.1515/psr-2017-0018.

[8] R. Sood, S. Cavaliere, D.J. Jones, J. Roziere, Electrospun nanofibre composite polymer electrolyte fuel cell and electrolysis membranes, Nano Energy 26 (2016) 729–745, https://doi.org/10.1016/j.nanoen.2016.06.027.

[9] K.D. Papadimitriou, F. Paloukis, S.G. Neophytides, J.K. Kallitsis, Cross-linking of side chain unsaturated aromatic polyethers for high temperature polymer electrolyte membrane fuel cell applications, Macromolecules 44 (2011) 4942–4951, https://doi.org/10.1021/ma200351z.

[10] M. Molleo, X. Chen, H.J. Ploehn, B.C. Benicewicz, High polymer content 2,5-pyridine-polybenzimidazole copolymer membranes with improved compressive properties, Fuel Cell. 15 (2015) 150–155, https://doi.org/10.1002/fuce.201400129.

[11] S.S. Rao, V.R. Hande, S.M. Sawant, S. Praveen, S.K. Rath, K. Sudarshan, D. Ratna, D. Patri, α-ZrP nanoreinforcement overcomes the trade-off between phosphoric acid dopability and thermomechanical properties: nanocomposite HTPEM with stable fuel cell performance, ACS Appl. Mater. Interfaces 11 (2019) 37013–37025, https://doi.org/10.1021/acsami.9b09405.

[12] D.E. Smith, D.A. Walsh, The nature of proton shuttling in protic ionic liquid fuel cells, Adv. Energy Mater. 9 (2019), 1900744, https://doi.org/10.1002/aenm.201900744.

[13] Y. Zhang, R. Xue, Y. Zhong, F. Jiang, M. Hu, Q. Yu, Nafion/IL intermediate temperature proton exchange membranes improved by mesoporous hollow silica spheres, Fuel Cell. 18 (2018) 389–396, https://doi.org/10.1002/fuce.201700228.
[14] V. Atanasov, A.S. Lee, E.J. Park, S. Maurya, E.D. Baca, C. Fujimoto, M. Hibbs, I. Matanovic, J. Kerres, Y.S. Kim, Synergistically integrated phosphonated poly (pentafluorostyrene) for fuel cells, Nat. Mater. 20 (2021) 370–377, https://doi.org/10.1038/s41563-020-00841-z.
[15] K. Kakinuma, H. Taniguchi, T. Asakawa, T. Miyao, M. Uchida, Y. Aoki, T. Akiyama, A. Masuda, N. Sato, A. Iiyama, The possibility of intermediate–temperature (120 °C)–Operated polymer electrolyte fuel cells using perfluorosulfonic acid polymer membranes, J. Electrochem. Soc. 169 (2022), 044522, https://doi.org/10.1149/1945-7111/ac624b.
[16] R. Sun, M. Agrawal, K.C. Neyerlin, J.D. Snyder, E.A. Elabd, Proton conducting sulfonated poly(ionic liquid) block copolymers, Macromolecules 55 (2022) 6716–6729, https://doi.org/10.1021/acs.macromol.2c00468.
[17] S.K. Jain, D. Rawlings, S. Antoine, S.A. Segalman, S. Han, Proton conducting sulfonated poly(ionic liquid) block copolymers, Macromolecules 55 (2022) 615–622, https://doi.org/10.1021/acs.macromol.1c01808.
[18] T. Stettner, A. Balducci, Protic ionic liquids in energy storage devices: past, present and future perspective, Energy Storage Mater. 40 (2021) 402–414, https://doi.org/10.1016/j.ensm.2021.04.036.
[19] T.L. Greaves, C.J. Drummond, Protic ionic liquids: evolving structure–property relationships and expanding applications, Chem. Rev. 115 (2015) 11379–11448, https://doi.org/10.1021/acs.chemrev.5b00158.
[20] H.A. Elwan, R. Thimmappa, M. Mamlouk, K. Scott, Applications of poly ionic liquids in proton exchange membrane fuel cells: a review, J. Power Sources 510 (2021), 230371, https://doi.org/10.1016/j.jpowsour.2021.230371.
[21] S. Kim, S. Kim, M. Park, Enhanced proton transport in nanostructured polymer electrolyte/ionic liquid membranes under water-free conditions, Nat. Commun. 1 (2010) 1–7, https://doi.org/10.1038/ncomms1086.
[22] J. Stoimenovski, E.I. Izgorodina, D.R. MacFarlane, Ionicity and proton transfer in protic ionic liquids, Phys. Chem. Chem. Phys. 12 (2010) 10341–10347, https://doi.org/10.1039/C0CP00239A.
[23] A.R. Hajipour, F. Rafiee, Acidic bronsted ionic liquids, Org. Prep. Proced. Int. 42 (2010) 285–362, https://doi.org/10.1080/00304948.2010.490177.
[24] L.E. Shmukler, M.S. Gruzdev, N.O. Kudryakova, Y.A. Fadeeva, A.M. Kolker, L. P. Safonova, Thermal behavior and electrochemistry of protic ionic liquids based on triethylamine with different acids, RSC Adv. 6 (2016) 109664–109671, https://doi.org/10.1039/C6RA21360J.
[25] M.S. Gruzdev, L.E. Shmukler, N.O. Kudryakova, A.M. Kolker, Y.A. Sergeeva, L. P. Safonova, Triethanolamine-based protic ionic liquids with various sulfonic acids: synthesis and properties, J. Mol. Liq. 242 (2017) 838–844, https://doi.org/10.1016/j.molliq.2017.07.078.
[26] T. Stettner, A. Balducci, Protic ionic liquids in energy storage devices: past, present and future perspective, Energy Storage Mater. 40 (2021) 402–414, https://doi.org/10.1016/j.ensm.2021.04.036.
[27] J. Rao, X. Wang, R. Yunis, V. Ranganathan, P.C. Howlett, D.R. MacFarlane, M. Forsyth, H. Zhu, A novel proton conducting ionogel electrolyte based on poly (ionic liquids) and protic ionic liquid, Electrochim. Acta 346 (2020), 136224, https://doi.org/10.1016/j.electacta.2020.136224.
[28] M. Isik, L. Porcarelli, N. Lago, H. Zhu, M. Forsyth, D. Mecerreyes, Proton conducting membranes based on poly(ionic liquids) having phosphonium counter-cations, Macromol. Rapid Commun. 39 (2018), 1700627, https://doi.org/10.1002/marc.201700627.
[29] G. Huang, H. Zhu, L. Porcarelli, Y. García, L.A. O'Dell, M. Forsyth, Study of ion transport in novel protic polymerized ionic liquids and composites, Macromol. Chem. Phys. 223 (2022), 2200124, https://doi.org/10.1002/macp.202200124.
[30] J. Guo, Z. Sun, Y. Zhou, F. Yan, Poly(ionic liquid)-based energy and electronic devices, chin, J. Chem. 40 (2022) 1099–1108, https://doi.org/10.1002/cjoc.202100820.
[31] G. Huang, L. Porcarelli, Y. Liang, M. Forsyth, H. Zhu, Influence of counteranion on the properties of polymerized ionic liquids/ionic liquids proton-exchange membranes, ACS Appl. Energy Mater. 4 (2021) 10593–10602, https://doi.org/10.1021/acsaem.1c01571.
[32] A. Fdz De Anastro, N. Lago, C. Berlanga, M. Galcerán, M. Hilder, M. Forsyth, D. Mecerreyes, Poly(ionic liquid) iongel membranes for all solid-state rechargeable sodium battery, J. Membr. Sci. 582 (2019) 435–441, https://doi.org/10.1016/j.memsci.2019.02.074.
[33] E. Mamontov, K.W. Herwig, A time-of-flight backscattering spectrometer at the Spallation Neutron Source, BASIS, Rev. Sci. Instrum. 82 (2011), 085109, https://doi.org/10.1063/1.3626214.
[34] R. Cubitt, G. Fragneto, D17: the new reflectometer at the ILL, Appl. Phys. A: Mater. Sci. Process. 74 (2002) s329–s331, https://doi.org/10.1007/s003390201611.
[35] Z.B. Zhou, H. Matsumoto, K. Tatsumi, Low-melting, low-viscous, hydrophobic ionic liquids: 1-alkyl(alkyl ether)-3-methylimidazolium perfluoroalkyltrifluoroborate, Chem. Eur J. 10 (2004) 6581–6591, https://doi.org/10.1002/chem.200400533.
[36] A.T. Tran, J. Tomlin, P.H. Lam, B.L. Stinger, A.D. Miller, D.J. Walczyk, O. Cruz, T. D. Vaden, L. Yu, Conductivity, viscosity, spectroscopic properties of organic sulfonic acid solutions in ionic liquids, ChemEng 3 (2019) 81, https://doi.org/10.3390/chemengineering3040081.
[37] Z.B. Zhou, H. Matsumoto, K. Tatsumi, Low-melting, low-viscous, hydrophobic ionic liquids: 1-alkyl(alkyl ether)-3-methylimidazolium perfluoroalkyltrifluoroborate, Chem. Eur J. 10 (2004) 6581–6591, https://doi.org/10.1002/chem.200400533.
[38] M. Anouti, M. Caillon-Caravanier, Y. Dridi, H. Galiano, D. Lemordant, Synthesis and characterization of new pyrrolidinium based protic ionic liquids. Good and superionic liquids, J. Phys. Chem. B 112 (2008) 13335–13343, https://doi.org/10.1021/jp805992b.
[39] A.B. Pereiro, J.M.M. Araújo, S. Martinho, F. Alves, S. Nunes, A. Matias, C.M. M. Duarte, L.P.M. Rebelo, I.M. Marrucho, Fluorinated ionic liquids: properties and applications, ACS Sustainable Chem. Eng. 1 (2013) 427–439, https://doi.org/10.1021/sc300163n.
[40] T. Yasuda, H. Kinoshita, M.S. Miran, S. Tsuzuki, M. Watanabe, Comparative study on physicochemical properties of protic ionic liquids based on allylammonium and propylammonium cations, J. Chem. Eng. Data 58 (2013) 2724–2732, https://doi.org/10.1021/je301284x.
[41] T.L. Greaves, C.J. Drummond, Protic ionic liquids: properties and applications, Chem. Rev. 108 (2008) 206–237, https://doi.org/10.1021/cr068040u.
[42] V. Jovanovski, R. Marcilla, D. Mecerreyes, Tuning the properties of functional pyrrolidinium polymers by (Co)polymerization of diallyldimethylammonium ionic liquids, macromol, Rapid Commun. 31 (2010) 1646–1651, https://doi.org/10.1002/marc.201000215.
[43] V. Jovanovski, G. Cabañero, H. Grande, D. Mecerreyes, Comparison between two different synthetic routes of pyrrolidinium functional polymeric ionic liquids, Macromol. Symp. 311 (2012) 77–82, https://doi.org/10.1002/masy.201000102.
[44] A.S. Shaplov, R. Marcilla, D. Mecerreyes, Recent advances in innovative polymer electrolytes based on poly(ionic liquid)s, Electrochim. Acta 175 (2015) 1834, https://doi.org/10.1016/j.electacta.2015.03.038.
[45] L.M. Timofeeva, Y.A. Vasilieva, N.A. Kleshcheva, D.A. Topchiev, Mechanism of interaction of diallylmethylamine and its protonated and quaternary forms with their own radicals in solvent, Russ. Chem. Bull. 48 (1999) 856–863, https://doi.org/10.1007/BF02494626.
[46] E. Lufrano, C. Simari, M.L. Di Vona, I. Nicotera, R. Narducci, How the morphology of nafion-based membranes affects proton transport, Polymers 13 (2021) 359, https://doi.org/10.3390/polym13030359.
[47] D.J.S. Patinha, L.C. Tomé, M. Isik, D. Mecerreyes, A.J.D. Silvestre, I.M. Marrucho, Expanding the applicability of poly(ionic liquids) in solid phase microextraction: pyrrolidinium coatings, Materials 10 (2017) 1094, https://doi.org/10.3390/ma10091094.
[48] S. Jeremias, M. Kunze, S. Passerini, M. Schönhoff, Polymerizable ionic liquid with state of the art transport properties, J. Phys. Chem. B 117 (2013) 10596–10602, https://doi.org/10.1021/jp407083z.
[49] A.H. Shah, J. Li, H. Yang, U.A. Rana, V. Ranganathan, H.M. Siddiqi, D. R. MacFarlane, M. Forsyth, H. Zhu, Enhancement of 'Dry' proton conductivity by self-assembled nanochannels in all-solid polyelectrolytes, J. Mater. Chem. A. 4 (2016) 7615–7623, https://doi.org/10.1039/C6TA00368K.
[50] Y. Schneider, M.A. Modestino, B.L. McCulloch, M.L. Hoarfrost, R.W. Hess, R. A. Segalman, Ionic conduction in nanostructured membranes based on polymerized protic ionic liquids, Macromolecules 46 (2013) 1543–1548, https://doi.org/10.1021/ma3024624.
[51] Y. Chen, M. Thorn, S. Christensen, C. Versek, A. Poe, R.C. Hayward, M. T. Tuominen, S. Thayumanavan, Enhancement of anhydrous proton transport by supramolecular nanochannels in comb polymers, Nat. Chem. 2 (2010) 503–508, https://doi.org/10.1038/nchem.629.
[52] M. Prager, A. Pawlukojc, A. Wischnewski, J. Wuttke, Inelastic neutron scattering study of methyl groups rotation in some methylxanthines, J. Chem. Phys. 127 (2007), 214509, https://doi.org/10.1063/1.2803187.
[53] F. Foglia, Q. Berrod, A.J. Clancy, K. Smith, G. Gebel, V. García Sakai, M. Appel, J. M. Zanotti, M. Tyagi, N. Nahmoudi, T.S. Miller, J.R. Varcoe, A.P. Perisamy, D.J. L. Brett, P.R. Shearing, S. Lyonnard, P. McMillan, Disentangling water, ion and polymer dynamics in an anion exchange membrane, Nat. Mater. 21 (2022) 555–563, https://doi.org/10.1038/s41563-022-01197-2.